JCBFM Open

Journal of Cerebral Blood Flow & Metabolism (2011), 1–12

www.jcbfm.com

Occlusion of cortical ascending venules causes blood flow decreases, reversals in flow direction, and vessel dilation in upstream capillaries

John Nguyen[1], Nozomi Nishimura[1], Robert N Fetcho[1], Costantino Iadecola[2] and Chris B Schaffer[1]

[1]*Department of Biomedical Engineering, Cornell University, Ithaca, New York, USA;* [2]*Department of Neurology and Neuroscience, Weill Cornell Medical College, New York, New York, USA*

The accumulation of small strokes has been linked to cognitive dysfunction. Although most animal models have focused on the impact of arteriole occlusions, clinical evidence indicates that venule occlusions may also be important. We used two-photon excited fluorescence microscopy to quantify changes in blood flow and vessel diameter in capillaries after occlusion of single ascending or surface cortical venules as a function of the connectivity between the measured capillary and the occluded venule. Clotting was induced by injuring the target vessel wall with femtosecond laser pulses. After an ascending venule (AV) occlusion, upstream capillaries showed decreases in blood flow speed, high rates of reversal in flow direction, and increases in vessel diameter. Surface venule occlusions produced similar effects, unless a collateral venule provided a new drain. Finally, we showed that AVs and penetrating arterioles have different nearest-neighbor spacing but capillaries branching from them have similar topology, which together predicted the severity and spatial extent of blood flow reduction after occlusion of either one. These results provide detailed insights into the widespread hemodynamic changes produced by cortical venule occlusions and may help elucidate the role of venule occlusions in the development of cognitive disorders and other brain diseases.
Journal of Cerebral Blood Flow & Metabolism (2011) **0,** 000–000. doi:10.1038/jcbfm.2011.95

Keywords: collateral flow; hemodynamics; nonlinear microscopy; stroke; vasoregulation

Introduction

There is increasing evidence that suggests cerebral venous insufficiency may have a role in many brain diseases. Small ischemic lesions in the cortical gray matter and in the periventricular and subcortical white matter have been linked to the development of cognitive dysfunction (Kovari *et al*, 2004; Mok *et al*, 2004; Vermeer *et al*, 2003). These lesions, which have previously been attributed to arteriolar clots or hemorrhages (Fisher, 1965), have recently also been found to correlate with venule pathology and occlusion (Black *et al*, 2009; Moody *et al*, 1995). Furthermore, venular occlusions have long been believed to have either a primary or secondary role in multiple sclerosis (Putnam, 1937; Singh and Zamboni, 2009). However, due in part to limitations of existing animal models of microvascular occlusion, very little is known about the impact of venule occlusions on cerebral hemodynamics.

Previous studies have focused on blood flow deficits resulting from thrombosis in large cerebral veins. Occlusion of the superior sagittal sinus (Ungersbock *et al*, 1993) and its bridging veins (Nakase *et al*, 1997*a*, *b*) in animal models caused severe blood flow reductions in underlying capillaries and resulted in ischemic infarction. Additional studies of occlusion of the superior sagittal sinus have shown that blood flow reductions were not as severe when more bridging veins were present, suggesting that vascular topology may be critical for blood flow redistribution (Ueda *et al*, 2000). Although these studies provide insights into the effects of thrombosis of larger-surface veins, the techniques used for blocking these large vessels do not translate to the production of clots in smaller ($<50\,\mu$m diameter) surface venules (SVs) or

Correspondence: Professor CB Schaffer, Department of Biomedical Engineering, Cornell University, Ithaca, NY 14853, USA.
E-mail: cs385@cornell.edu
JN received a fellowship from the NSF GK-12 program (0841291); NN received a postdoctoral grant from the National Institutes of Health (1F32AG031620-01A2), American Heart Association (09POSST2550177), and a L'Oréal USA Fellowship for Women in Science; CI received funding from the National Institute of Health (NS37853); and CBS received funding from the American Heart Association (0735644T) and the Ellison Medical Foundation (AG-NS-0330-06).
Received 18 April 2011; revised 3 June 2011; accepted 8 June 2011

in ascending venules (AVs). The recent finding that femtosecond laser ablation (Vogel *et al*, 2005) can be used to initiate clotting in individual vessels has permitted targeted occlusion of single cortical penetrating arterioles (PAs) (Nishimura *et al*, 2007, 2010) and capillaries (Nishimura *et al*, 2006). This nonlinear optical technique is an ideal tool for producing occlusions in targeted cortical venules to investigate whether small venule clots in the cerebral vasculature lead to physiologically important blood flow deficits.

In this study, we quantified the effects of single venule occlusions on blood flow in the rat neocortex. We used femtosecond laser ablation to damage the endothelium and induce clotting in targeted venules and used two-photon excited fluorescence (2PEF) microscopy to investigate the resulting blood flow and vessel diameter changes as a function of both topological separation and spatial distance from the occluded vessel. We found that occlusion of a single AV caused dramatic decreases in blood flow and increases in vessel diameter in capillaries that were upstream from the targeted venule. Similar results were observed after the occlusion of a SV, but flow decreases were almost eliminated when a surface collateral vessel that provided a new drain was present. We mapped the cortical microvascular topology in $600 \times 600 \times 500\,\mu m^3$-sized volume and used these data to predict the spatial extent and severity of blood flow reduction after an AV occlusion and found these predictions to agree well with *in vivo* measurements. These results highlight the dominant influence of vascular topology in determining blood flow rearrangements that result from a vascular occlusion and provide the first comprehensive, quantitative picture of blood flow rearrangements that result from venular occlusions in the neocortex.

Materials and methods

Animals and Surgical Procedures

Experiments were performed on 27 male Sprague Dawley rats (Harlan Inc., South Easton, MA, USA) ranging from 265 to 375 g in mass. Ascending venule occlusions were induced in 16 animals, SV occlusions were induced in 8 animals (with collateral vessel: 3, no collateral: 5), and the rest were used in sham experiments. Only one venule was occluded in each animal. All rats were anesthetized with urethane (1.5 g/kg rat), and glycopyrolate (0.5 mg/kg rat) was administered intramuscularly to help prevent secretions. Body temperature was kept at 37°C using a heating blanket controlled by a rectal thermometer (50-7053; Harvard Apparatus, Holliston, MA, USA). Heart rate and arterial oxygen saturation were monitored using a pulse oximeter (MouseOx; Starr Life Sciences Corp., Oakmont, PA, USA) clipped to the rat's hind paw. Hydration was maintained with hourly subcutaneous injections of 5% glucose (wt/vol) in saline (1 mL/kg rat). Physiologic parameters were manually recorded every 20 minutes to ensure that the physiologic state of the rat was stable.

Craniotomies were performed to gain optical access to the brain. A subcutaneous injection 0.1 mL bupivicaine (0.125% wt/vol in deionized water) was administered to reduce pain at the incision site. A $\sim 3 \times 6\,mm^2$ craniotomy was made over the parietal cortex and the dura was removed. The brain was then covered in 1.5% agarose (A9793; Sigma, St Louis, MO, USA) in artificial cerebral spinal fluid (Kleinfeld and Delaney, 1996), and an 8-mm diameter no. 1.5 glass coverslip (50201; World Precision Instruments, Sarasota, FL, USA) was placed over the craniotomy and sealed using dental cement (Co-Oral-Ite Dental Mfg Co.). To visualize the vasculature using 2PEF microscopy, we intravenously injected ~ 0.3 mL of 5% (wt/vol) 2-MDa fluorescein-conjugated dextran (FD2000S; Sigma) in saline. All animal care and experimental procedures were approved by the Institutional Animal Care and Use Committee of Cornell University.

Two-Photon Imaging of the Cortical Vasculature

In vivo images were obtained using a custom-designed 2PEF microscope that used a low-energy, 100-fs, 800-nm, 76-MHz repetition rate pulse train generated by a Ti:sapphire oscillator (Mira-HP; Coherent Inc., Santa Clara, CA, USA) that was pumped by a continuous wave diode-pumped solid state laser (Verdi-V18; Coherent Inc.). Data acquisition and laser scanning were controlled using MPSCOPE software (Nguyen *et al*, 2006). Fluorescence was detected through an interference filter centered at 517 nm with a 65-nm bandpass. A 0.28 numerical aperture, $\times 4$ magnification, air objective (Olympus, Center Valley, PA, USA) was used to obtain images of the entire cranial window. In these large-area 2PEF images, surface vessels were identified and large venules were followed upstream to identify candidate AVs and SVs for occlusion (Figure 1A). A 0.95 numerical aperture, $\times 20$ magnification, water-immersion objective (Olympus) was used for high-resolution imaging (Figure 1B), measurements of vessel diameter, and blood flow speed (Figure 1C), and vessel occlusion (Figure 2).

The vasculature surrounding the target venule was mapped with 1-μm-spaced image stacks. These high-resolution image stacks were used to map the topological relationship and spatial distance between measured vessels and the targeted venule (Figure 1B). Diameters were measured by averaging at least 10 movie frames and manually selecting a segment of the vessel. The selected region was then thresholded (20% of maximum intensity), and the average width across the length of the selected segment was calculated as the vessel diameter (Figure 1Ci). Centerline red blood cell (RBC) velocities were obtained by tracking the motion of RBCs, which do not take up the intravenously injected dye and show up as dark patches inside the vessel (Figure 1Cii). Repetitive linescans along the axis of the vessel, at a rate of 1.7 kHz for ~ 1 minute, were used to form a space-time image in which moving RBCs produce streaks with a slope that is equal to the inverse of the speed (Figure 1Ciii; characteristic diameter

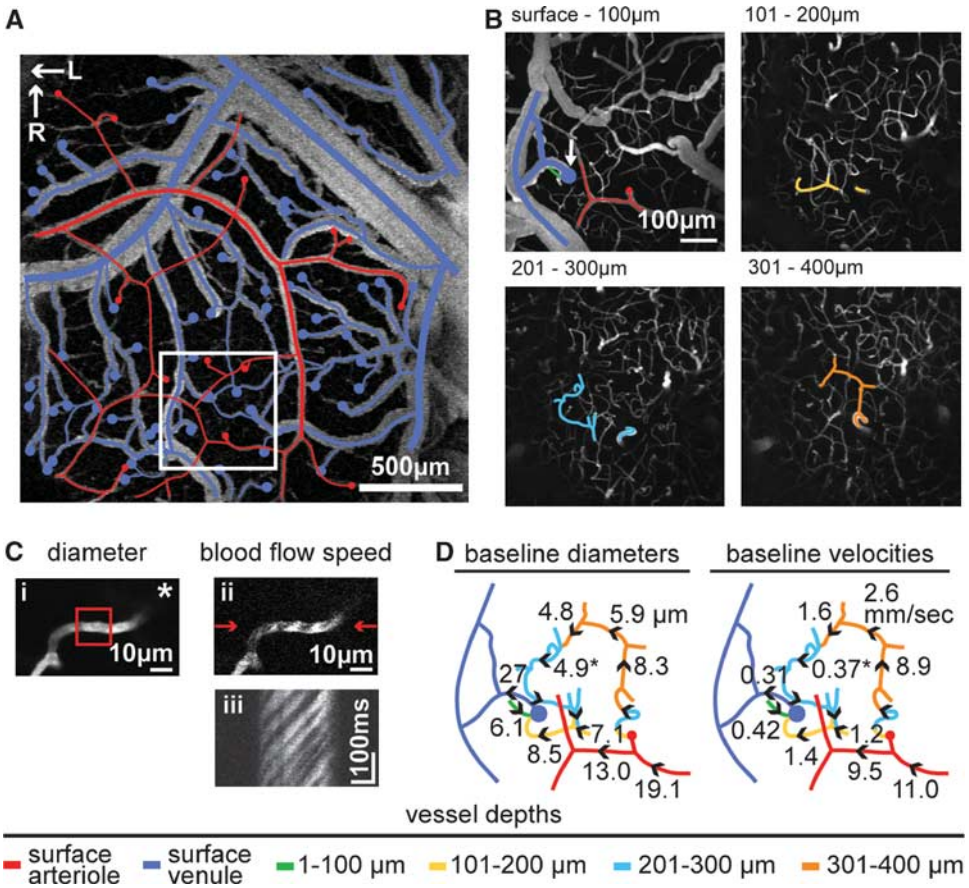

Figure 1 2PEF microscopy to map connectivity in the rat cortical vasculature and measure vessel diameter and blood flow velocity in individual vessels. (**A**) Averaged projection of a 2PEF image stack of fluorescently labeled vasculature. Surface (penetrating) arterioles and surface (ascending) venules are indicated with red and blue lines (circles), respectively. The white box indicates the magnified region shown in **B**. Arrows labeled R and L indicate rostral and lateral directions, respectively. (**B**) Series of 100-μm-thick average projections of a 2PEF image stack starting from the brain surface to a depth of 400 μm. In each image projection, selected surface and subsurface vessels are outlined, indicating the vascular network in which vessel diameter and blood flow velocity were quantified. White arrow indicates the targeted AV. (**C**) Averaged 2PEF image of an individual capillary used to measure vessel diameter (i) along a selected segment (red box), single 2PEF image frame of red blood cells flowing through a capillary, with arrows indicating the path of the linescan (ii), and the corresponding space-time image from a linescan from which the blood flow speed can be determined (iii). (**D**) Baseline diameter and blood flow speed measurements of the vascular network traced in panel **B**, where arrows indicate blood flow direction and the asterisk-marked value corresponds to the capillary measured in panel **C**. Color coding indicates the vessel depth. The occlusion of the AV in this network and the resulting changes in vessel diameter and blood flow are shown in Figures 2 and 3, respectively. AV, ascending venule; 2PEF, two-photon excited fluorescence.

and RBC flow speed of all measured vessels shown in Supplementary Figure 1). The slope was calculated using an automated image-processing algorithm (Schaffer *et al*, 2006). Measured parameters were then mapped to vascular networks that included the targeted venule (Figure 1D).

Vessel Identification

Ascending venules were defined as vertically oriented, subsurface vessels that transported blood from the capillary bed to the brain surface, as confirmed through measurement of blood flow direction. Vessels directly downstream from AVs and on the brain surface were defined as SVs. Surface arterioles, which form a net-like network on the brain surface, as well as PAs, which transport blood vertically into the brain, were also identified (Figure 1A). The PAs fed an extensive network of capillaries that eventually connected to and drained into AVs. We defined all subsurface vessels between a PA and an AV as capillaries. We determined the dependence of blood flow and vessel diameter changes after venule occlusion on topological separation by counting the number of vessel branches between a measured vessel and the occluded venule. Measured capillaries that could not be traced back to the targeted venule were grouped as 'not connected'.

For this study, we occluded individual AVs and SVs. For SV experiments, we found two topologically distinct vascular patterns for SVs immediately upstream from AVs. Both patterns were composed of two AVs that merged into one SV, forming a 'Y'-shaped architecture (outlined in blue; Figures 5A and 5B). The two patterns were distinguished by the presence or absence of a 'collateral'

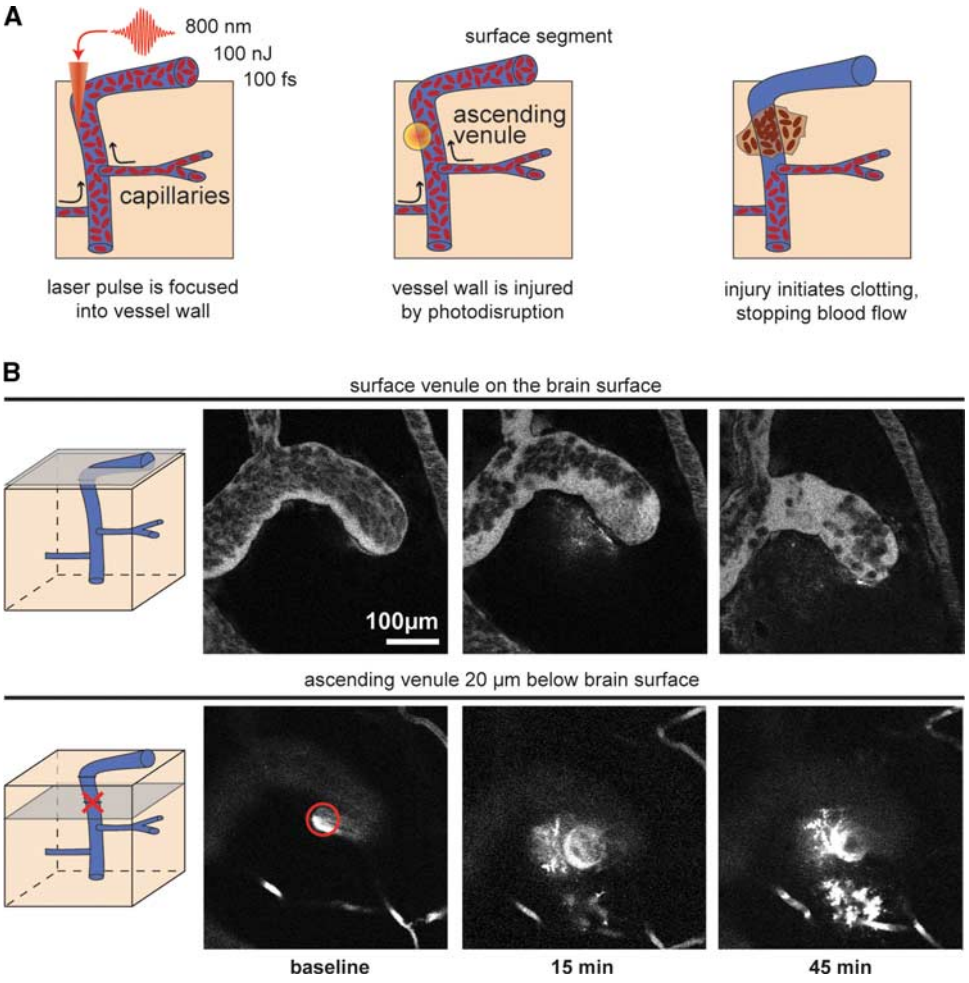

Figure 2 Targeted occlusion of cortical ascending venules through clotting initiated by femtosecond laser photodisruption. (**A**) Schematic of venule clotting process. (**B**) Example of an AV occlusion. Gray planes in schematics on the left indicate the imaging plane, with the red 'X' indicating the location of the targeted ablation in the AV. Images on the right show a time-lapse series of the surface segment (top) and the 20-μm deep ascending segment (bottom) of the target vessel during clotting. This example shows clotting of an AV by ablation of the ascending segment of the vessel, approximately halfway between the first branching capillary and the brain surface. At baseline, flow of red blood cells was evident in the ascending and surface segments of the targeted venule. The vessel wall of the ascending segment was irradiated with 100-nJ pulses, until we observed extravasation of fluorescently labeled blood plasma, indicating that the vessel wall was injured (15 minutes). Further damage was induced along the vessel wall until a clot formed and complete cessation of red blood cell motion in the ascending and surface segments was observed (45 minutes). Nearby surface vessels were not clotted and remained flowing. AV, ascending venule.

SV that connected to another SV (purple line and dashed blue lines, respectively; Figure 5A). In both topologies, occlusions were induced in the merged venule (red circles; Figures 5A and 5B) and vessel diameter and blood flow measurements were made in upstream SVs and capillaries.

Targeted Clotting of Venules by Femtosecond Laser Ablation

Femtosecond laser pulses were tightly focused on the wall of the targeted vessel (characteristic diameter and RBC flow speed of target venules shown in Supplementary Figure 2), causing nonlinear absorption of laser energy that drives photodisruptive damage (Nishimura *et al*, 2006). This injury initiated the natural clotting cascade, forming a clot that stopped blood flow in the targeted venule (Figure 2A). As nonlinear absorption occurred only at the focus at which laser intensity was the highest, photodisruption was confined to the focal volume, leaving the surrounding vessels and tissues intact. Venules were irradiated with a 50-fs, 800-nm, 1-kHz pulse train produced by a Ti:sapphire regenerative amplifier (Legend 1k USP; Coherent Inc.) pumped by a Q-switched laser (Evolution 15; Coherent Inc.) and seeded by a Ti:sapphire oscillator (Chinhook Ti:sapphire laser; Kapteyn-Murnane Laboratories Inc., Boulder, CO, USA, pumped by Verdi-V6; Coherent Inc.). Both 2PEF imaging and ablation laser beams were combined along the same beam path using a polarizer beam splitter within the custom 2PEF microscope and focused to the same plane, allowing for simultaneous imaging and ablation (Nishimura *et al*, 2006). Pulse energy for ablation was varied with neutral density filters, and the number of pulses focused in the vessel lumen was

controlled using a mechanical shutter with a 2-millisecond minimum opening time (VMM-D4; Uniblitz, Rochester, NY, USA). For AV occlusions, the targeted segment was always located above the first branching upstream capillary and below the brain surface, at a depth of several tens of micrometers. Initially, venules were irradiated with a single pulse with energy below the expected damage threshold ($\sim$100 nJ at a depth of $\sim$50 μm). The number of pulses was then increased from a single pulse to 1,000 pulses, by increments of 100, until damage was observed, which was indicated by extravasation of fluorescently labeled plasma outside the vessel. If no injury was observed, the energy was increased by $\sim$25% and the process was repeated. Once extravasation occurred, the vessel was irradiated at multiple locations along the lumen until the motion of RBCs ceased and an accumulation of RBCs in the targeted vessel segment was observed (Figure 2). The procedure for occluding SVs was similar, except that the initial laser energies used were lower because the target vessel was located on the brain surface.

Characterization of Capillary Topology and Prediction of Spatial Dependence of Blood Flow Change After Penetrating Arteriole or Ascending Venule Occlusion

Two-photon excited fluorescence image stacks from six additional rats were used to quantify the locations of AVs and PAs over $\sim$4 mm^2 of brain surface (Figure 6A) and determine the nearest-neighbor separations (Supplementary Figure 7). In three animals, we traced the connectivity of all vessels within a $\sim$0.1-mm^3 volume of brain tissue using custom software (Figure 6B). From these data, we quantified the distance between capillary segments and the nearest AV (2,153 capillaries) or PA (2,203 capillaries) as a function of the number of branches upstream or downstream the capillary was from the AV or PA (Figure 6C). We then determined the distribution of capillary branch numbers as a function of distance from PAs and AVs in 50-μm radial bins. We used *in vivo* flow change data from this study for AV occlusions and from previous work for PA occlusions (Nishimura *et al*, 2010) to determine the average blood flow decrease in different capillary branches stemming from an occluded AV or PA. Combining both the capillary branch number distribution (Figure 6C) and this flow change data, we predicted the postclot blood flow speed change as a function of distance from occluded AVs and PAs (Figure 6D). A step-by-step overview of the procedure for generating data in Figure 6D is given in the Supplementary Text.

Statistical Analysis

Boxplots were generated with Matlab (The Mathworks, Natick, MA, USA) using the boxplot function (Figures 4A, 4E, 5C, and 5E). The dependence of median RBC flow speed change (Figure 4B), reversal rate (Figure 4D), and mean vessel dilation (Figure 4F) in capillaries as a function of distance from occluded AVs were determined using a variable-width spatial window that was constrained to contain 20 data points. Trend lines were further smoothed with a 20-μm moving average and a running 95% confidence interval about the trend line was calculated.

Differences were considered significant for P-values < 0.05. For nonparametric data, rank-based analysis was conducted using Dwass–Steel–Critchlow–Fligner (StatsDirect, Altrincham, Cheshire, UK) multiple comparisons test (Figures 4A and 5C), whereas normally distributed data were analyzed using the Tukey–Kramer (StatsDirect) multiple comparisons test (Figures 4E, 5E, and 7B). For binomial data, statistical differences were calculated using a binomial proportions test with a Bonferroni adjustment (Figures 4C and 5D). Medians are reported for nonparametric data, whereas means are reported for normal data.

Results

We used 2PEF imaging of fluorescently labeled blood plasma in anesthetized rats to map vascular topology and quantify blood flow speed and vessel diameter in surface vessel and capillary networks near AVs and SVs that were candidates for occlusion (Figure 1). Irradiation of the targeted venules with high-energy, tightly focused, femtosecond laser pulses caused localized vascular injury, leading to extravasation of fluorescently labeled plasma and RBCs and triggering clotting of the vessel (Figure 2). Nearby surface vessels and capillaries were not clotted and remained flowing. We then measured the changes in diameter and RBC centerline velocity that resulted from venule occlusion in individual vessels throughout the nearby vascular network (Figure 3, Supplementary Figures 3 and 4).

Ascending Venule Occlusions Caused Decreased Blood Flow Speeds in Upstream Capillaries

To understand the impact of AV occlusions on blood flow in nearby and connected blood vessels, we investigated how changes in blood flow speed depend on the topological connection and spatial distance between individual vessels and the occluded venule. The RBC speed in capillaries that were one to four branches upstream from the clotted venule decreased dramatically, with flow speeds of only 6% (16%) of the baseline value for vessels one (two) branch(es) upstream from the occlusion (Figure 4A). The average speed did not change in capillaries that were more than four branches upstream or not connected to the occluded venule, although vessels five to seven branches upstream showed a 9.5 times increased variance in speed after the occlusion when compared with sham experiments (Figure 4A; $P < 1.0\text{E-}7$, F-test). Surface venules downstream from the occluded venule slowed, whereas parallel SVs (i.e., vessels that drained into the same venule as the clotted vessel) did not change speed (Figure 4A). The median RBC speed in measured capillaries located within 100 μm of the occluded venule decreased to $\sim$26% of the baseline value, and returned to baseline with increasing distance from the occluded vessel (Figure 4B).

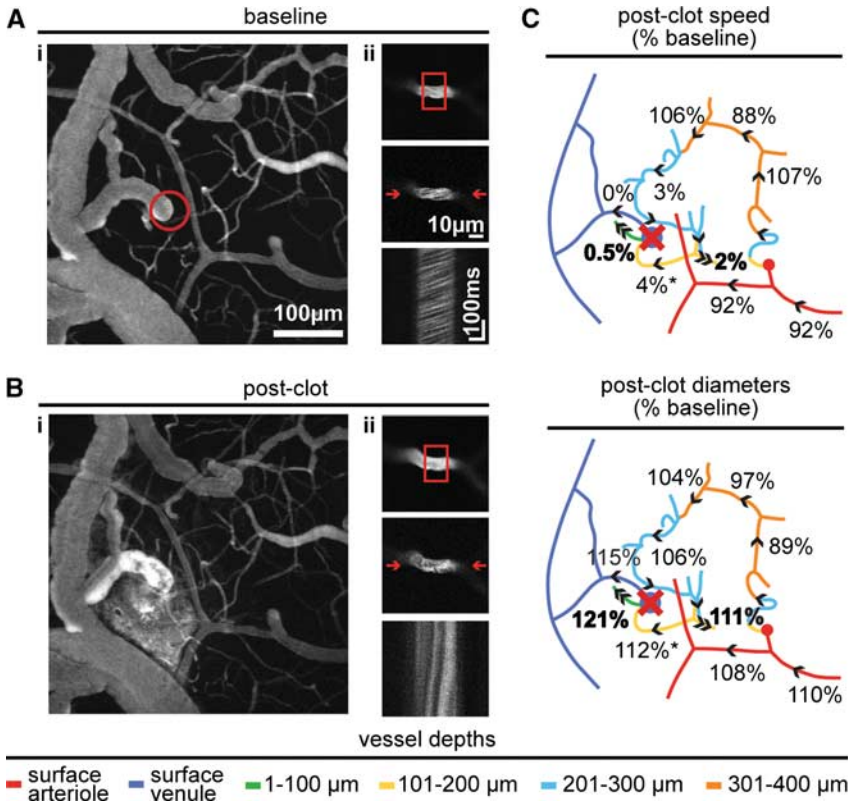

Figure 3 Measurements of changes in RBC speed and vessel diameter in capillaries upstream from an occluded ascending venule. 2PEF imaging at (**A**) baseline and (**B**) after clotting a single AV showing: (i) average projection of 100-μm deep image stack of fluorescently labeled vasculature and (ii) image data for measurements of the diameter and RBC speed in an individual capillary. Extravasation of fluorescently labeled blood plasma was visible near the clotted venule in **B**(i), but the nearby surface vasculature and underlying capillaries remained intact. There was a slight dilation in the capillary shown in **A**(ii) and **B**(ii) after the clot, and the postclot linescan showed more vertically oriented streaks from moving RBCs, indicating dramatically decreased blood flow speed. (**C**) Vessel RBC speeds (top) and diameters (bottom) in the vascular network after occlusion of an AV, expressed as a percentage of the baseline values. Vessels topologically close to the targeted venule slowed dramatically, 2 of the 10 measured vessels reversed flow direction (indicated with double arrows and bold numerical values), and the majority of vessels increased in diameter. Red 'X' indicates the location of the clotted AV. The vessel marked with an asterisk corresponds to the vessel in **A**(ii) and **B**(ii). The clotting sequence for this AV is shown in Figure 2. AV, ascending venule; RBC, red blood cell; 2PEF, two-photon excited fluorescence.

Blood Flow Directions Reversed in Many Upstream Capillaries After Ascending Venule Occlusions

In addition to changes in blood flow speed, we observed dramatic changes in the routing of blood flow through the capillary bed after AV occlusion. We frequently observed a reversal in blood flow direction in capillaries one to four branches upstream from the occluded venule, with just over half of the first and second upstream branches reversing flow direction (Figure 4C). Neither capillaries not connected to the occluded venule nor downstream or parallel SVs reversed flow direction (Figure 4C). The number of blood flow reversals in capillaries decreased with increasing distance from the occluded venule, with no flow reversals observed $>650\,\mu$m away from the target vessel (Figure 4D).

The Diameter of Upstream Capillaries Increased After Ascending Venule Occlusions

We further examined the impact of AV occlusions on the diameter of nearby and connected vessels. We found that capillaries up to three branches upstream from the targeted venule dilated after the clot as compared with sham experiments, with an average diameter increase of $\sim$25% (Figure 4E). Capillaries further upstream or not connected to the targeted vessel, as well as downstream and parallel SVs, did not dilate significantly (Figure 4E). The amount of dilation decreased with increasing distance from the clot, with no dilation observed at distances $>200\,\mu$m (Figure 4F).

Collateral Surface Venules, When Present, Helped Maintain Normal Blood Flow After Surface Venule Occlusions

We also examined the blood flow changes caused by occlusion of SVs in vascular topologies that had (Figure 5A; Supplementary Figure 5) and did not have (Figure 5B; Supplementary Figure 6) a collateral SV. On average, blood flow speeds in capillaries one and two branches upstream from the AVs

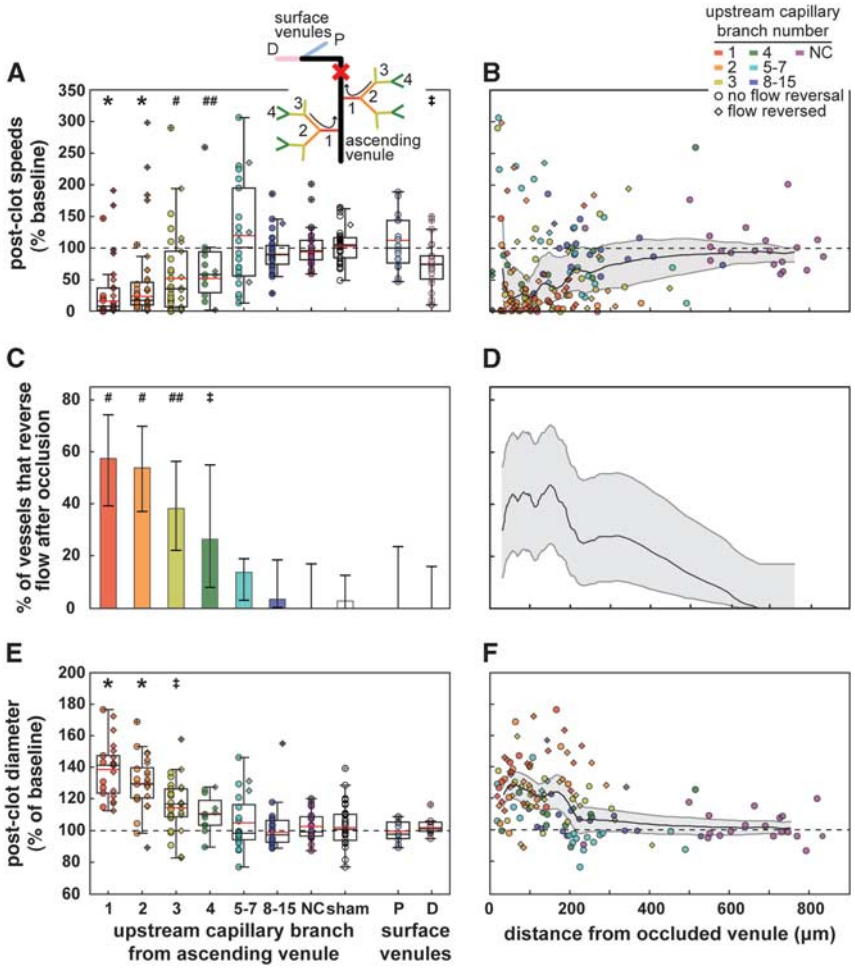

Figure 4 Ascending venule occlusions resulted in decreased blood flow, reversals of flow direction, and increased vessel diameter in upstream capillaries. (**A**, **C** and **E**) Changes in RBC speed (expressed as percentage of baseline speed), blood flow direction (percentage of vessels with reversed flow), and vessel diameter (percentage of baseline diameter), respectively, after an AV occlusion for upstream capillaries and downstream surface venules as a function of topological connection to the occluded vessel. The schematic inset shows the vessel enumeration scheme, with arrows indicating the direction of blood flow at baseline and the red 'X' indicating the occlusion location. (**B**, **D** and **F**) Changes in RBC speed, blood flow direction, and vessel diameter, respectively, as a function of distance away from the occluded AV for capillaries. The black line in panel **B** (**F**) represents a running median (mean), whereas the line in panel **D** represents a running fraction. Capillaries topologically grouped in 'NC' indicate that no connection to the target vessel was able to be determined, and 'sham' indicates experiments in which no vessel was clotted. P and D represent parallel and downstream surface venules, respectively. In speed and diameter plots, diamonds (circles) indicate vessels in which flow did (did not) reverse direction after the occlusion. Black and red lines in the boxplots represent the median and mean, respectively. Statistical outliers, denoted with a crosshair, were excluded when calculating the mean. Color coding to indicate topological connectivity is the same for all applicable panels. Gray-shaded regions in panels **B**, **D**, and **F** indicate 95% confidence intervals about their respective trend lines. Three outlier points are not shown (groups: 4, sham, P; 5.9, 6.1, 5.2, respectively) in panels **A** and **B**. $^{*}P < 1.0\text{E-}7$, $^{\#}P < 0.0005$, $^{\#\#}P < 0.005$, $^{\ddagger}P < 0.05$; compared with sham vessels. AV, ascending venule; NC, not connected; RBC, red blood cell.

were unaffected by a SV occlusion when a collateral vessel was present, whereas flow was reduced to an average of 12% of the baseline speed when no collateral vessel was present (Figure 5C). Blood flow reversals in the first two upstream capillaries occurred only when no collateral vessel was present (Figure 5D). Diameters increased in the first upstream capillary branch only when no collateral vessel was present, whereas the second upstream capillary branch dilated after a SV occlusion both with and without a collateral (Figure 5E).

Topological Architecture had a Large Role in Determining Blood Flow Changes

To gain insights into the role of vascular topology in determining blood flow rearrangements after an occlusion, we used *in vivo* imaging to map the vascular topology over $\sim 0.1\,\text{mm}^3$ volumes in the cortex and combined this with topology-dependent measurements of RBC speed change after vascular occlusion to predict the spatial extent and severity of blood flow decrease. We found that the number of AVs outnumbered PAs by a factor of 1.8 (Figure 6A;

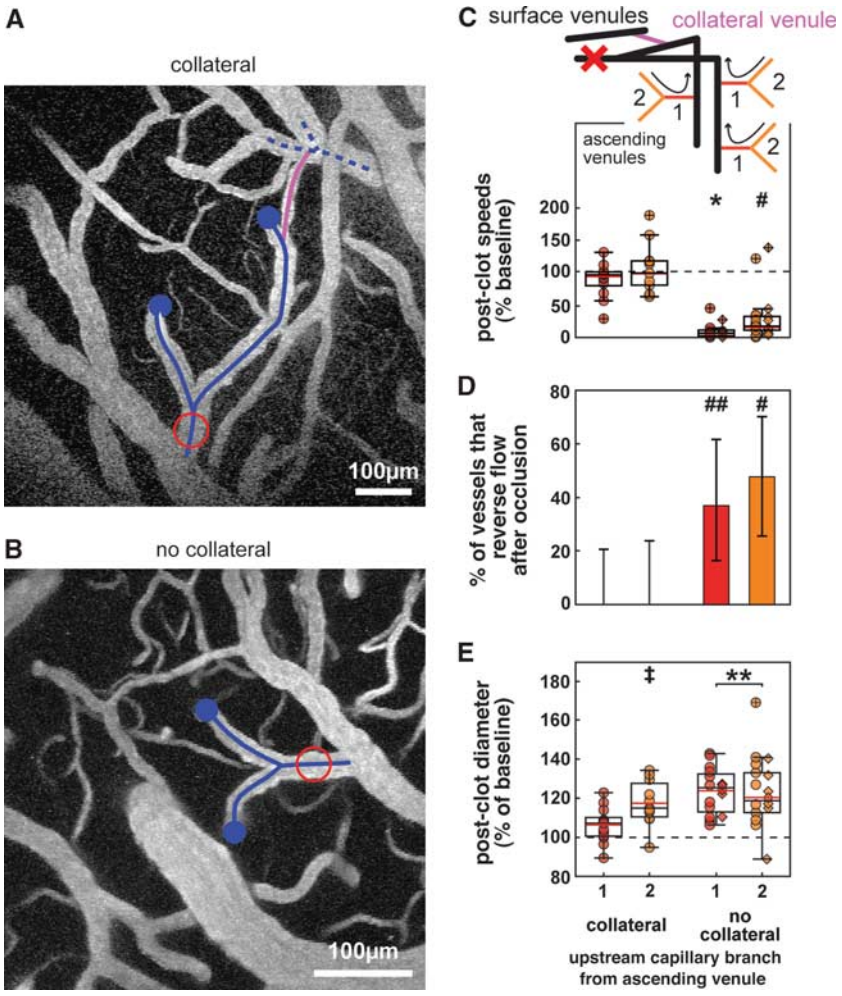

Figure 5 Collateral surface venules helped maintain normal flow in upstream capillaries after surface venule occlusions. Averaged projections of 2PEF image stacks of brain surface vasculature with (**A**) a collateral vessel (purple) links a terminal venule to another draining surface venule (dashed) or (**B**) with no such collateral vessel. The red circle indicates the clot location. Maps of the flow changes in the upstream vessels after occlusion are shown in Supplementary Figures 5 and 6. (**C**) RBC speed in upstream capillaries, expressed as a percentage of the baseline values, for clots placed in surface venules with and without a collateral vessel. Schematic inset indicates the vascular topology considered, vessel designations, and location of the surface venule occlusion. (**D**) Percentage of capillaries that reverse flow direction after surface venule occlusions. (**E**) Plot of the vessel diameter, expressed as a percentage of the baseline value, for capillaries upstream from clots formed in surface venules. Diamonds (circles) indicate vessels in which flow did (did not) reverse direction after the occlusion and the color-coding scheme is the same for all plots. $^{*}P < 1.0E\text{-}7$, $^{**}P < 0.00001$, $^{\#}P < 0.0005$, $^{\#\#}P < 0.005$, $^{\ddagger}P < 0.05$; compared with sham vessels. RBC, red blood cell; 2PEF, two-photon excited fluorescence.

Supplementary Figure 7; 6 animals, 360 PAs to 201 AVs). We used tracings of all vessels (Figure 6B; 4,256 capillaries in 3 animals) to determine the three-dimensional spatial location of each capillary as a function of topological connectivity to the nearest AV or PA. The average distance of capillaries from an AV or PA as a function of the number of branches upstream or downstream, respectively, was comparable (Figure 6C), suggesting a similarity in the capillary branching topology away from AVs and PAs. We then used *in vivo* measurements of capillary flow speed decreases after AV and PA occlusions as a function of topological separation from Figure 4A and from the study by Nishimura *et al* (2010), respectively, to calculate the postclot flow speed changes in capillaries as a function of distance from the occluded vessel, weighted according to the topological data from Figure 6C. This calculation predicted both the spatial extent and the severity of the blood flow deficit to be smaller after occlusion of a single AV as compared with a PA (Figure 6D), in agreement with the experimental data from Figure 4B and previous work (Nishimura *et al*, 2007, 2010).

Discussion

We examined vessel-by-vessel hemodynamics after cortical venule occlusions using nonlinear optical techniques. Measurements of centerline RBC speed and direction, vessel diameter, and topological

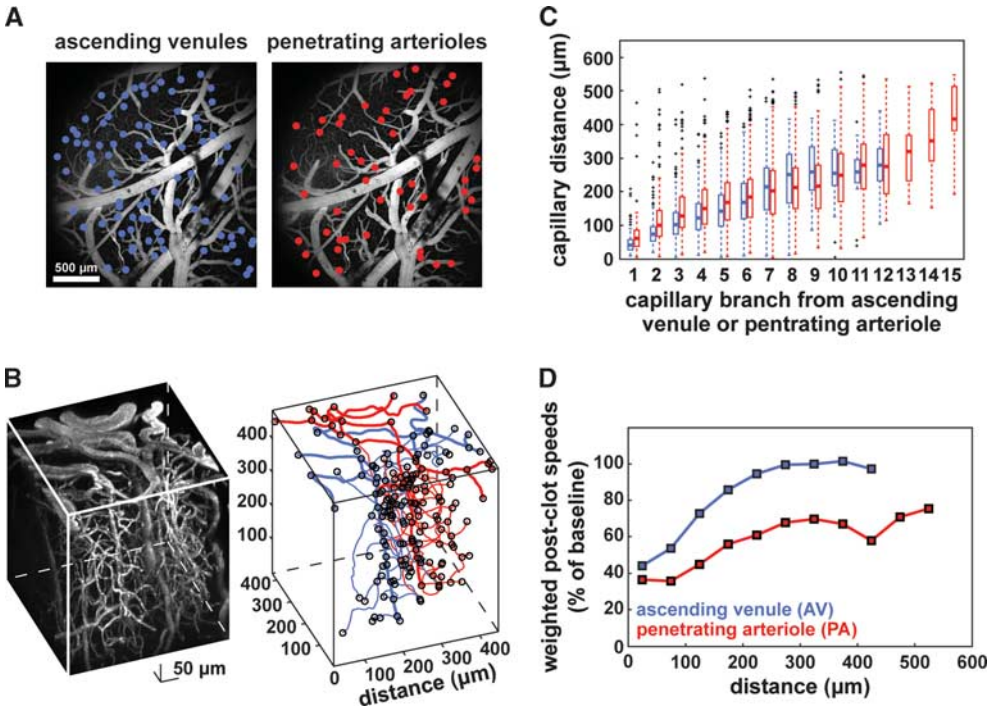

Figure 6 Differences in flow changes resulting from ascending venule and penetrating arteriole occlusions are a consequence of different AV–AV and PA–PA spacing together with similar capillary topologies. (**A**) Average projections of a 2PEF image stack of the cortical surface vasculature. Locations of AVs (left) and PAs (right) are indicated by blue and red dots, respectively. (**B**) 2PEF, three-dimensional volumetric projection, using Voxx (Clendenon *et al*, 2002), of cortical vasculature starting at the brain surface (left). All vessels and bifurcation points were traced to characterize vascular topology. Surface vessels and a subset of the traced capillaries are shown (right) to emphasize the complexity of the cortical vasculature. (**C**) Boxplot of capillary distance to nearest AV (blue) or PA (red) as a function of capillary branches away from an AV or a PA. (**D**) A weighted calculation of postclot speeds as a function of distance for occlusion of an AV (blue) and PA (red) using *in vivo* flow data that were topologically weighted based on the data in panel **C**. Each data point represents a weighted mean for a 50-μm-binned window. AV, ascending venule; PA, penetrating arteriole; 2PEF, two-photon excited fluorescence.

connectivity of individual vessels were obtained using 2PEF microscopy and femtosecond laser ablation was used to trigger clotting in targeted AVs and SVs. Vessels were measured before and after the occlusion to determine topologically and spatially dependent changes in RBC speed and direction, as well as in vessel diameter. Capillaries immediately upstream from the target venule experienced a dramatic decrease in RBC speed, reversals in blood flow direction, and an increase in diameter, with each parameter recovering to baseline values in vessels further upstream from the clotted venule. Similar behaviors were observed in upstream capillaries after SV occlusions in topologies that did not contain a collateral vessel, whereas blood flow deficits were alleviated with the presence of a surface collateral venule. Furthermore, we studied the density of AVs and PAs, as well as the topology of the capillaries that branch from them and used these values to predict differences in the spatial extent and severity of the blood flow decreases that result from AV and PA occlusions. These observations revealed the blood flow impact, both as a function of vascular topology and distance through the cortex, associated with cortical venule occlusions.

Nonlinear Optical Techniques Enable the Creation of Robust Models of Small Cortical Venule Occlusion

The ability to measure cerebral blood flow during normal and pathologic states is critical for the development of an animal model of venule stroke. Most previous work on cortical venule occlusions has used laser Doppler flowmetry to characterize flow changes that result from occlusion of cortical veins with $\sim$0.1 to 1 mm diameter (Nakase *et al*, 1997*a*, *b*; Ungersbock *et al*, 1993; Ueda *et al*, 2000). Although this approach allows for mapping of regional blood flow changes resulting from large vessel occlusions, it would tend to average over the effects associated with occlusions in vessels with $\sim$10 to 50 μm diameter, such as those considered in this study. Quantitative autoradiography has also been used to map tissue perfusion deficits after superior sagittal sinus occlusion (Kurokawa *et al*, 1990), but this method does not enable the *in vivo* measurements that could, e.g., connect vascular topology to blood flow change. In this study, we used 2PEF microscopy to characterize, at the vessel-by-vessel level, changes in blood flow and diameter in vessels located deep within the cortical tissue

after venule occlusion. Although it is difficult to characterize a large number of vessels in one experiment with this approach, the limited topological and spatial extent of blood flow rearrangements we observed after AV and SV occlusion suggest that 2PEF imaging is well suited to the study of these microvessel occlusions (Zhang and Murphy, 2007). Other methods that enable simultaneous measurement of blood flow changes across many surface or penetrating/ascending vessels, such as Doppler optical coherence tomography (Srinivasan *et al*, 2011) or advanced intrinsic optical imaging (Chen *et al*, 2011), could complement the approach taken here.

Conventional methods for producing vascular occlusions are not well suited to producing occlusions in small venules. Mechanical ligation approaches are limited to large vessels, such as the superior sagittal sinus (Frerichs *et al*, 1994). Optical methods relying on linear excitation of an intravenously injected photosensitizer (Watson *et al*, 1985) potentially provide higher precision (Nakase *et al*, 1997*a*), but thrombus formation is difficult to localize to a single vessel. Embolus injection models have been used to occlude smaller vessels (Miyake *et al*, 1993), but this technique is inappropriate for venule occlusions, as the emboli will block arterioles and capillaries before ever reaching the venous system. In this study, we tightly focused high-energy, femtosecond laser pulses onto the vessel lumen to drive nonlinear absorption of the laser energy at the focus, thereby inducing an injury that is confined within the focal volume (Nishimura *et al*, 2006). This injury triggers clotting in the target vessel, while leaving nearby vessels and the surrounding brain tissue intact (see Supplementary Movie 1). Overall, this approach provides a robust animal model of cortical venule occlusions that allows precise and controlled clotting of single venules at and below the brain surface with minimal collateral damage.

Topology is a Dominant Factor in the Redistribution of Blood After Vascular Occlusion

Vascular topology has a crucial role in redistributing blood flow after a cortical vessel clot. Occlusion of communicating surface arterioles does not lead to severe decreases in flow in downstream arterioles and capillaries because the vascular anastomoses within the surface arteriole network provide collateral flow (Blinder *et al*, 2010; Schaffer *et al*, 2006). Similarly, after occlusion of a SV with a collateral vessel, we find that blood flow changes in upstream capillaries are minimized, whereas topologies that do not contain a surface collateral venule result in severe blood flow decreases. These studies highlight the important role of redundancy in both the arterial and the venular networks in maintaining flow after surface vessel occlusions. In contrast, occlusions in vessels with topologies that contain no collateral pathways, such as PAs and AVs, lead to flow decreases in the underlying capillaries. Clotting of a PA results in severe decreases in blood flow in downstream capillaries to at least seven branches downstream from the targeted vessel (Nishimura *et al*, 2010), whereas blood flow is seen to recover after the fourth branch upstream after an AV occlusion. The difference in the topological distance through the capillary network at which blood flow recovers after a PA or AV occlusion can be attributed to the fact that PAs are outnumbered by AVs almost two to one. As the capillary branching pattern is similar for both vessel types, this difference in density, and therefore in distance between two PAs or two AVs (Supplementary Figure 7), suggests that the number of capillary branches between two PAs is greater than the number of branches between two AVs. As a result, blood flow deficits in capillaries downstream from an occluded PA will extend further into the capillary network before another nearby PA is able to effectively provide alternatively sourced blood flow. In contrast, because two AVs are closer, blood in capillaries upstream from an occluded AV requires fewer branches to reach an alternative AV, resulting in less severe blood flow deficits. To further support this idea, we performed a topology-weighted analysis of capillary flow changes as a function of distance from an occluded vessel, which showed that the spatial extent and severity of blood flow decrease was less dramatic after an AV occlusion as compared with a PA occlusion. Taken together, these results not only implicate the role of vascular topology and connectivity in the redistribution of blood flow but also highlight the importance of the occlusion location within the vascular hierarchy.

Capillary Dilations are a Passive Process After an Ascending Venule Occlusion

One of the key findings in this study is the large dilation in upstream capillaries after occlusion of an AV. One question is whether the observed dilation is an active or passive process. Previous anatomic studies of the cerebral microvasculature have established the lack of smooth muscle cells in the capillaries upstream from AVs (Rhodin, 1968), suggesting that capillaries do not actively modulate their diameter. This leads to the hypothesis that the capillary dilations we observe are a passive process, induced by an increase in intravascular pressure, caused by the fact that after the venule occlusion, the immediately upstream capillaries are now topologically further away from a low pressure draining venule. To model this scenario, we considered the capillary as a tube embedded in a matrix of brain tissue (Fung *et al*, 1966), with a Young's modulus, E, of 1.5 kPa and a Poisson's ratio, v, of 0.5 (Gefen *et al*, 2003). The change in vessel radius, R, is then linked to the change in intravascular pressure, P, by

$$P_c - P_o = \left(\frac{E}{1+v}\right)\left(\frac{R_c - R_o}{R_o}\right) \quad (1)$$

where P_c and R_c are postclot and P_o and R_o the

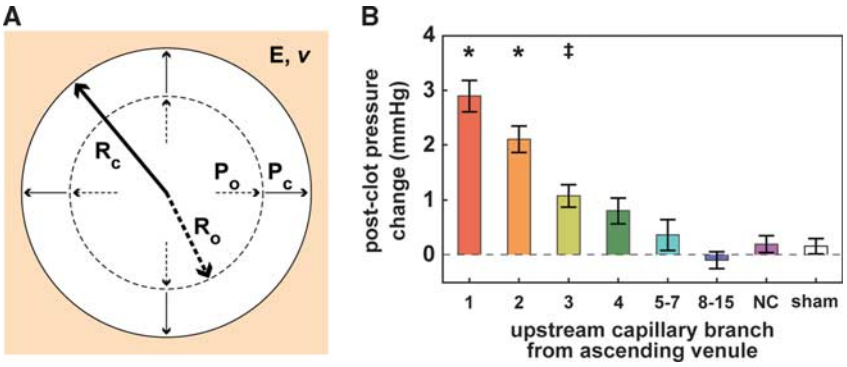

Figure 7 Post-occlusion dilation in upstream capillaries was attributed to an increase in internal pressure. (**A**) Schematic of capillary located within the brain tissue that possesses a Young's modulus, E, and Poisson's ratio, v. At baseline, the initial radius and pressure is R_o and P_o, respectively, both of which increase to R_c and P_c, respectively, after the clot. (**B**) Bar plot of the change (mean ± s.e.m.) in intraluminal pressure as a function of topological connection to the occluded vessel calculated from equation (1) and the mean diameter changes in Figure 4E. $^*P < 1.0E\text{-}7$, $^‡P < 0.05$; compared with sham vessels.

baseline pressure and radius, respectively. Using equation (1), we calculated the pressure increase required to induce a dilation that agrees with our experimental measurements (Figure 7). The 5% to 10% increase in intravascular pressure we calculate compares well with the pressure difference measured between capillary beds and the first draining venules in cat mesentery (Lipowsky, 2005). However, we note that pericytes have been shown to actively modulate the diameter of capillaries (Peppiatt *et al*, 2006), and their involvement in the diameter changes observed here cannot be ruled out, although the magnitude of the dilation we observed is larger than the typical diameter changes associated with pericyte activation (Fernandez-Klett *et al*, 2010). Indeed, previous work showed capillaries downstream from an occluded PA dilate (Nishimura *et al*, 2010), presumably an active process, with diameter changes smaller than those observed here.

Blood Flow Decreases After Small Venule Strokes may be Damaging to Brain Cells

The extensive blood flow and vascular changes we observed after occlusion of single cortical AVs and SVs suggest that these occlusions may lead to dysfunction in brain cells. Previous work has shown that occlusion of large cortical veins leads to regional reductions in blood flow that causes ischemic infarction (Nakase *et al*, 1997*b*). We found that blood flow decreased to ~20% of baseline values within 100 μm of occluded AVs, which is at the level at which cellular inhibition of protein synthesis and energy failure begins to occur (Mies *et al*, 1991). These blood flow reductions are not sufficient to cause acute cell death, but, if protracted in time, may lead to brain dysfunction (Iadecola, 2010). This conclusion is supported by studies in the intestinal mesenteric circulation showing that venular occlusion lead to parenchymal cell death that increased with time (Takase *et al*, 1999). Furthermore, changes in vascular wall shear stress caused by changes in flow speed and direction could promote inflammation and oxidative stress in endothelial cells (Harrison *et al*, 2006). Finally, increased intravascular capillary pressures may lead to increased blood–brain barrier permeability (Mayhan *et al*, 1986), which can cause brain edema and inflammation (Mayhan *et al*, 1986; Rosenberg, 1999). Venous insufficiently has been associated with an increasing number of brain pathologies, ranging from multiple sclerosis to dementia (Black *et al*, 2009; Moody *et al*, 1995; Singh and Zamboni, 2009). Although the role of venous alterations in the pathogenesis of these conditions remains uncertain, these results show that venular occlusions have profound and widespread effects on brain microcirculation, highlighting the pathogenic potential of venous insufficiency.

Disclosure/conflict of interest

The authors declare no conflict of interest.

References

Black S, Gao F, Bilbao J (2009) Understanding white matter disease: imaging-pathological correlations in vascular cognitive impairment. *Stroke* 40:S48–52

Blinder P, Shih AY, Rafie C, Kleinfeld D (2010) Topological basis for the robust distribution of blood to rodent neocortex. *Proc Natl Acad Sci USA* 107:12670–5

Chen BR, Bouchard MB, McCaslin AF, Burgess SA, Hillman EM (2011) High-speed vascular dynamics of the hemodynamic response. *Neuroimage* 54:1021–30

Clendenon JL, Phillips CL, Sandoval RM, Fang SF, Dunn KW (2002) Voxx: a PC-based, near real-time volume rendering system for biological microscopy. *Am J Physiol-Cell Ph* 282:C213–8

Fernandez-Klett F, Offenhauser N, Dirnagl U, Priller J, Lindauer U (2010) Pericytes in capillaries are contractile *in vivo*, but arterioles mediate functional hyperemia in the mouse brain. *Proc Natl Acad Sci USA* 107:22290–5

Fisher CM (1965) Lacunes: small, deep cerebral infarcts. *Neurology* 15:774–84

Frerichs KU, Deckert M, Kempski O, Schurer L, Einhaupl K, Baethmann A (1994) Cerebral sinus and venous thrombosis in rats induces long-term deficits in brain-function and morphology—evidence for a cytotoxic genesis. *J Cereb Blood Flow Metab* 14:289–300

Fung YC, Zweifach BW, Intaglie M (1966) Elastic environment of capillary bed. *Circ Res* 19:441–61

Gefen A, Gefen N, Zhu QL, Raghupathi R, Margulies SS (2003) Age-dependent changes in material properties of the brain and braincase of the rat. *J Neurotraum* 20:1163–77

Harrison DG, Widder J, Grumbach I, Chen W, Weber M, Searles C (2006) Endothelial mechanotransduction, nitric oxide and vascular inflammation. *J Intern Med* 259:351–63

Iadecola C (2010) The overlap between neurodegenerative and vascular factors in the pathogenesis of dementia. *Acta Neuropathol* 120:287–96

Kleinfeld D, Delaney KR (1996) Distributed representation of vibrissa movement in the upper layers of somatosensory cortex revealed with voltage-sensitive dyes. *J Comp Neurol* 375:89–108

Kovari E, Gold G, Herrmann FR, Canuto A, Hof PR, Michel JP, Bouras C, Giannakopoulos P (2004) Cortical microinfarcts and demyelination significantly affect cognition in brain aging. *Stroke* 35:410–4

Kurokawa Y, Hashi K, Okuyama T, Uede T (1990) Regional ischemia in cerebral venous hypertension due to embolic occlusion of the superior sagittal sinus in the rat. *Surg Neurol* 34:390–5

Lipowsky HH (2005) Microvascular rheology and hemodynamics. *Microcirculation* 12:5–15

Mayhan WG, Faraci FM, Heistad DD (1986) Disruption of the blood-brain barrier in cerebrum and brain stem during acute hypertension. *Am J Physiol* 251:H1171–5

Mies G, Ishimaru S, Xie Y, Seo K, Hossmann KA (1991) Ischemic thresholds of cerebral protein-synthesis and energy-state following middle cerebral-artery occlusion in rat. *J Cereb Blood Flow Metab* 11:753–61

Miyake K, Takeo S, Kaijihara H (1993) Sustained decrease in brain regional blood-flow after microsphere embolism in rats. *Stroke* 24:415–20

Mok VC, Wong A, Lam WW, Fan YH, Tang WK, Kwok T, Hui AC, Wong KS (2004) Cognitive impairment and functional outcome after stroke associated with small vessel disease. *J Neurol Neurosurg Psychiatry* 75:560–6

Moody DM, Brown WR, Challa VR, Anderson RL (1995) Periventricular venous collagenosis—association with leukoaraiosis. *Radiology* 194:469–76

Nakase H, Kempski OS, Heimann A, Takeshima T, Tintera J (1997*a*) Microcirculation after cerebral venous occlusions as assessed by laser Doppler scanning. *J Neurosurg* 87:307–14

Nakase H, Nagata K, Ohtsuka H, Sakaki T, Kempski O (1997*b*) An experimental model of intraoperative venous injury in the rat. *Skull Base Surg* 7:123–8

Nguyen QT, Tsai PS, Kleinfeld D (2006) MPScope: a versatile software suite for multiphoton microscopy. *J Neurosci Meth* 156:351–9

Nishimura N, Rosidi NL, Iadecola C, Schaffer CB (2010) Limitations of collateral flow after occlusion of a single cortical penetrating arteriole. *J Cereb Blood Flow Metab* 30:1914–27

Nishimura N, Schaffer CB, Friedman B, Lyden PD, Kleinfeld D (2007) Penetrating arterioles are a bottleneck in the perfusion of neocortex. *Proc Natl Acad Sci USA* 104:365–70

Nishimura N, Schaffer CB, Friedman B, Tsai PS, Lyden PD, Kleinfeld D (2006) Targeted insult to subsurface cortical blood vessels using ultrashort laser pulses: three models of stroke. *Nat Methods* 3:99–108

Peppiatt CM, Howarth C, Mobbs P, Attwell D (2006) Bidirectional control of CNS capillary diameter by pericytes. *Nature* 443:700–4

Putnam TJ (1937) Lesions of 'encephalomyelitis' and multiple sclerosis—venous thrombosis as the primary alteration. *J Am Med Assoc* 108:1477–80

Rhodin JA (1968) Ultrastructure of mammalian venous capillaries, venules, and small collecting veins. *J Ultrastruct Res* 25:452–500

Rosenberg GA (1999) Ischemic brain edema. *Prog Cardiovasc Dis* 42:209–16

Schaffer CB, Friedman B, Nishimura N, Schroeder LF, Tsai PS, Ebner FF, Lyden PD, Kleinfeld D (2006) Two-photon imaging of cortical surface microvessels reveals a robust redistribution in blood flow after vascular occlusion. *Plos Biol* 4:258–70

Singh AV, Zamboni P (2009) Anomalous venous blood flow and iron deposition in multiple sclerosis. *J Cereb Blood Flow Metab* 29:1867–78

Srinivasan VJ, Atochin DN, Radhakrishnan H, Jiang JY, Ruvinskaya S, Wu W, Barry S, Cable AE, Ayata C, Huang PL, Boas DA (2011) Optical coherence tomography for the quantitative study of cerebrovascular physiology. *J Cereb Blood Flow Metab* 31:1339–45

Takase S, Delano FA, Lerond L, Bergan JJ, Schmid-Schonbein GW (1999) Inflammation in chronic venous insufficiency: is the problem insurmountable? *J Vasc Res* 36:3–10

Ueda K, Nakase H, Miyamoto K, Otsuka H, Sakaki T (2000) Impact of anatomical difference of the cerebral venous system on microcirculation in a gerbil superior sagittal sinus occlusion model. *Acta Neurochir (Wien)* 142:75–82

Ungersbock K, Heimann A, Kempski O (1993) Cerebral blood flow alterations in a rat model of cerebral sinus thrombosis. *Stroke* 24:563–9; discussion 9–70

Vermeer SE, Prins ND, den Heijer T, Hofman A, Koudstaal PJ, Breteler MM (2003) Silent brain infarcts and the risk of dementia and cognitive decline. *N Engl J Med* 348:1215–22

Vogel A, Noack J, Huttman G, Paltauf G (2005) Mechanisms of femtosecond laser nanosurgery of cells and tissues. *Appl Phys B-Lasers O* 81:1015–47

Watson BD, Dietrich WD, Busto R, Wachtel MS, Ginsberg MD (1985) Induction of reproducible brain infarction by photochemically initiated thrombosis. *Ann Neurol* 17:497–504

Zhang SX, Murphy TH (2007) Imaging the impact of cortical microcirculation on synaptic structure and sensory-evoked hemodynamic responses *in vivo*. *Plos Biol* 5:1152–67

Supplementary Information accompanies the paper on the Journal of Cerebral Blood Flow & Metabolism website (http://www.nature.com/jcbfm)